

Improved lower bound on superluminal quantum communication

Bruno Cocciaro,^{*} Sandro Faetti,[†] and Leone Fronzoni[‡]

Department of Physics Enrico Fermi, Università di Pisa, Largo Pontecorvo 3, 56127 Pisa, Italy



(Received 26 January 2018; published 23 May 2018)

As shown by Einstein, Podolsky, and Rosen (the EPR paradox) [A. Einstein, B. Podolsky, and N. Rosen, *Phys. Rev.* **47**, 777 (1935)], quantum mechanics is a nonlocal theory contrarily to what happens for any other modern physical theory. Alternative local theories based on superluminal communications have been also proposed in the literature. So far, no evidence for these superluminal communications has been obtained and only lower bounds for the superluminal velocities have been established. In this paper we describe an improved experiment that increases by about two orders of magnitude the maximum detectable superluminal velocities. The locality, the freedom of choice, and the detection loopholes are not addressed here. No evidence for superluminal communications has been found and a higher lower bound for their velocities has been established.

DOI: [10.1103/PhysRevA.97.052124](https://doi.org/10.1103/PhysRevA.97.052124)

I. INTRODUCTION

Einstein *et al.* [1] showed that orthodox quantum mechanics is a nonlocal theory [the Einstein-Podolsky-Rosen (EPR) paradox]. Consider, for instance, photons a and b in Fig. 1 that propagate in opposite directions and are in the polarization entangled state

$$|\psi\rangle = \frac{1}{\sqrt{2}}(|H, H\rangle + |V, V\rangle), \quad (1)$$

where H and V denote horizontal and vertical polarization, respectively. The entangled state represents a very special state that has no equivalent in classical and semiclassical physics. In particular, before a polarization measurement, the entangled photons cannot be represented in terms of two standard photons having a definite polarization (linear, circular, or elliptical polarization). Whatever the orientation of the absorption polarizer P_A (or P_B) is, the probability that photon a (or b) passes through the corresponding polarizer is $P = 1/2 = \text{const}$ for any polarizer orientation. Furthermore, according to quantum mechanics, if one photon first passes through polarizer P_A in Fig. 1 having the polarization axis at angle α with respect to the horizontal axis and is detected by the photon counter, the entangled state in Eq. (1) collapses instantaneously to the unentangled state $|\alpha_a, \alpha_b\rangle = |\alpha_a\rangle|\alpha_b\rangle$, where $|\alpha_a\rangle$ and $|\alpha_b\rangle$ denote single-photon states linearly polarized at the same angle α . Then, if polarizers P_A and P_B are oriented at angles α and ξ and one photon passes through polarizer P_A (or P_B), the probability that the other photon passes through polarizer P_B (or P_A) is $\bar{P}(\alpha, \xi) = \cos^2(\alpha - \xi)$ and the probability that both photons pass through both polarizers is $P(\alpha, \xi) = \frac{1}{2} \cos^2(\alpha - \xi)$. Then, according to quantum mechanics, the polarization measurement at point A or B affects instantaneously the result of the polarization measurement at point B or A whatever

distance d_{AB} between the polarizers is. In our experiment we use absorption polarizers and thus, if the photon encounters the polarizer, the quantum state collapses to a quantum mixture of a vacuum state (absorbed photon) and a linearly polarized state (transmitted photon). Then, if the photon is detected by the photon counter, one can infer that it was already linearly polarized just after exiting from the polarizer. Therefore, we assume here that the collapse of the polarization state occurs at the polarizers and not at the detectors.

The behavior predicted by quantum mechanics (spooky action at a distance) is reminiscent of the action at a distance that was introduced in the old physics but that has been completely rejected by the modern general relativity and electromagnetic theories. For this reason, Einstein *et al.* believed that quantum mechanics is a not complete theory and suggested that a complete theory should contain some additive local variables. According to these local models, the two entangled photons would be generated at point O in Fig. 1, each in a well-defined polarization state depending on the values of some unknown local variables. The probabilistic behavior that characterizes quantum mechanics would be a direct consequence of our lack of knowledge of these local variables. Before 1964, the choice between orthodox quantum mechanics and local variable models was only a subject of philosophical debate, but Bell [2] demonstrated that any theory based on local variables must satisfy an inequality (Bell inequality) that is violated by quantum mechanics. Then, no local variable model can entirely reproduce quantum mechanics and a direct experimental comparison between quantum mechanics theory and local variable models becomes possible.

Analogous inequalities have been found by Clauser *et al.* [3,4] (the Clauser-Horne-Shimony-Holt inequality). The experiment of Aspect *et al.* [5] clearly demonstrated that the Bell inequality is violated and also showed that quantum correlations cannot be explained in terms of subluminal or luminal communications between entangled particles. Many other experiments confirmed the Aspect *et al.* results and some recent experiments finally closed also the residual loopholes [6–9].

^{*}b.cocciaro@comeg.it

[†]sandro.faetti@unipi.it

[‡]leone.fronzoni@unipi.it

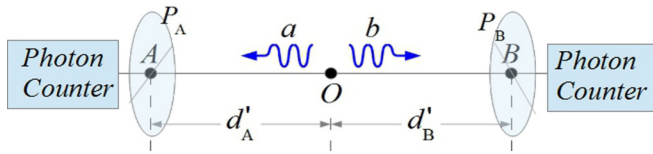


FIG. 1. Two entangled photons a and b are generated at O and get the absorption polarizing films P_A (Alice polarizer) and P_B (Bob polarizer). The photons passing through the polarizers are collected by photon-counting modules. With d'_A and d'_B we denote the optical paths of photons a and b from source O to polarizers P_A and P_B , respectively.

According to Gisin [10], in all sciences, except in quantum mechanics, correlations between events occurring at different places in the space have always been explained in terms of two basic mechanisms: common causes or communication. The EPR experiment of Aspect *et al.* and the most recent ones clearly exclude the common cause explanation (local variables) but also the possibility of any communication via subluminal signals. In order to not give up the principle of locality, J. Bell, in the interview reported at pages 45–47 in Ref. [11], suggested that these correlations could be due to superluminal communications and, subsequently, Eberhard [12] and Bohm and Hiley [13] developed well-defined and sound superluminal models based on this idea (v -causal models in the current literature [10]). To avoid causal paradoxes, a preferred frame must exist where superluminal signals propagate isotropically with unknown velocity $v_t = \beta_t c$ ($\beta_t > 1$). Below we will always define the relativistic parameter $\beta_t = v_t/c$ as the adimensional velocity. The existence of a preferred frame may be surprising, but Refs. [14,15] strongly stressed that a preferred frame is not in contrast to relativity. Furthermore, it should be noted that a universal preferred frame has been already observed: It is the cosmic microwave background frame that moves with the adimensional velocity $\beta \approx 10^{-3}$ with respect to the earth's geocentric frame. Of course, the cosmic microwave background frame would represent a good candidate as a preferred frame for superluminal communications. For a system made of only two entangled particles, it has been shown that superluminal communications between entangled particles could not be used to exchange information in the macroscopic word (signaling), but an important theorem was recently demonstrated [16,17]: Superluminal models allow signaling if more than two entangled particles are involved. Although one of us believes that signaling is not incompatible with relativity [14,15], most physicists think that there is no compatibility and that the experimental evidence of signaling would need a revision of relativity.

In the following we do not assume a specific superluminal model but we restrict our attention to all the possible models, as well as the Eberhard one, where a first event (the passage of a photon through a polarizer) affects a second event (the passage of a photon through the other polarizer) through superluminal communication. Furthermore, since we use absorption polarizers, we assume that the collapse of the state occurs when photons get to the polarizers. To have a naive idea of a superluminal mechanism, suppose that the passage of photon a through polarizer P_A does not induce the instantaneous collapse of the state of both photons to the

linearly polarized states $|\alpha_a\rangle$ and $|\alpha_b\rangle$ as predicted by quantum mechanics but only the local collapse of the state of photon a to $|\alpha_a\rangle$. The collapse of the second photon to the linear polarized state $|\alpha_b\rangle$ predicted by quantum mechanics will occur only when a collapsing superluminal wave reaches it. The collapsing wave propagates isotropically in the preferred frame at the adimensional superluminal velocity β_t ($\beta_t > 0$) and is created where (and when) the first event occurs (e.g., the first photon hits the polarizer). The first event is the one which occurs temporally before in the preferred frame. Starting from a similar idea, a rigorous model was developed by Eberhard [12] but, according to him, it represents only a possible example. Of course, in the limit $\beta_t \rightarrow \infty$, the collapse tends to be instantaneous everywhere and thus the superluminal models give the same results of quantum mechanics in this limit case. However, if the communication velocity has a high but finite value, it can occur that the second particle reaches its measurement device (the polarizer) when the collapsing wave has not yet reached it. In these special cases, the nonlocal quantum mechanics predictions cannot be satisfied and thus the Bell inequality should always be satisfied. Consider, for instance, the ideal case where polarizers P_A and P_B are at the same distances d'_A and d'_B in the preferred frame and thus the two photons get to the polarizers simultaneously (here we disregard, for simplicity, the width of the photons' wave packets, which will be taken into account below). In this ideal case, the probability $P(\alpha, \xi)$ cannot be given by the nonlocal quantum mechanics prediction $P(\alpha, \xi) = \frac{1}{2} \cos^2(\alpha - \xi)$ and the Bell inequality has to be satisfied. To verify this behavior, one can measure the Bell-Clauser-Horne-Shimony-Holt correlation parameter S_{\max} defined as [18,19]

$$S_{\max} = P_0 - \sum_{i=1}^3 P_i, \quad (2)$$

with $P_0 = P(45^\circ, 67.5^\circ)$, $P_1 = P(0^\circ, 67.5^\circ)$, $P_2 = P(45^\circ, 112.5^\circ)$, and $P_3 = P(90^\circ, 22.5^\circ)$. It has been demonstrated that, for any local variable model, S_{\max} must satisfy the modified Bell-Clauser-Horne-Shimony-Holt inequality $S_{\max} \leq 0$ [18,19], while quantum mechanics predicts $S_{\max} = \frac{(\sqrt{2}-1)}{2} \approx 0.2071$ for the entangled state in Eq. (1). Probabilities $P(\alpha, \xi)$ can be experimentally obtained using the relation

$$P(\alpha, \xi) = \frac{N(\alpha, \xi)}{N_{\text{tot}}}, \quad (3)$$

where $N(\alpha, \xi)$ are the coincidences between entangled photons passing through the polarizers during the acquisition time $\delta_a t$ and N_{tot} is the total number of entangled photons couples that can be obtained using

$$N_{\text{tot}} = \sum_{i=0}^3 N_i, \quad (4)$$

where $N_0 = N(0^\circ, 0^\circ)$, $N_1 = N(0^\circ, 90^\circ)$, $N_2 = N(90^\circ, 0^\circ)$, and $N_3 = N(90^\circ, 90^\circ)$. If $d'_A = d'_B$ in the preferred frame, the quantum predictions cannot be satisfied and S_{\max} should always satisfy the inequality $S_{\max} \leq 0$ [3,4,18,19]. However, due to the experimental uncertainty of the equalization of the optical paths and to the finite width of the photons' wave packets impinging on the polarizers, the arrival times of

photons at the polarizers cannot be exactly equalized and could differ by the quantity $\Delta t' = \frac{\Delta d'}{c}$, where $\Delta d'$ represents the uncertainty on the effective optical path difference that takes into account the uncertainty of the optical path difference but also any other source of spatial uncertainty that affects $\Delta t'$ [see Eq. (7) in [19]]. Thus, a superluminal communication would be impossible only if $\Delta t'$ is lower than the time $d'_{AB}/\beta_t c$ that is needed to establish communication between A and B , where d'_{AB} is the effective optical path from A to B in the preferred frame (see Fig. 1). The condition $\Delta t' < d'_{AB}/\beta_t c$ is satisfied only if β_t is lower than a maximum detectable adimensional velocity $\beta_{t,\max} = \frac{d'_{AB}}{\Delta d'}$. Therefore, due to the $\Delta d'$ uncertainty, a breakdown of quantum predictions ($S_{\max} < 0$) could be observed in the preferred frame only if the superluminal velocity satisfies the condition $\beta_t < \beta_{t,\max}$. In the laboratory earth frame the analysis becomes much more complex. Indeed, a time difference $\Delta t'$ in the preferred frame is related to the corresponding Δt in the laboratory frame by

$$\Delta t' = \gamma(\Delta t - \vec{\beta} \cdot \vec{AB}), \quad (5)$$

where $\vec{\beta}$ is the unknown adimensional relative velocity vector of the preferred frame with respect to the laboratory frame and \vec{AB} is the vector connecting points A and B . Then $\Delta t = 0$ in the laboratory frame does not imply $\Delta t' = 0$ except if $\vec{\beta} \cdot \vec{AB} = 0$ in Eq. (5). If the AB segment is east-west aligned, due to the earth's rotation around its axis, there are two times t_1 and t_2 for each sidereal day where \vec{AB} becomes orthogonal to $\vec{\beta}$ whatever the orientation of the $\vec{\beta}$ vector is [20,21]. At these times, if the superluminal adimensional velocity β_t is lower than $\beta_{t,\max}$, the predictions of quantum mechanics should be not satisfied and S_{\max} should exhibit a breakdown from the quantum value $S_{\max} = 0.2071$ toward $S_{\max} \leq 0$. However, a finite acquisition time δ_{at} has to be spent to measure the parameter S_{\max} and thus the orthogonality condition $\vec{\beta} \cdot \vec{AB} = 0$ can only be approximately satisfied during the entire acquisition time. Then, according to Eq. (5), the uncertainty $\Delta t'$ of the arrival times of the entangled photons at the two polarizers in the preferred frame is due to the uncertainty Δt of the arrival times in the laboratory frame and to the nonvanishing contribution $\vec{\beta} \cdot \vec{AB} \neq 0$ due to the finite acquisition time. Then, in the earth experiment, the maximum detectable velocity $\beta_{t,\max}$ is affected both by the uncertainty Δd of the equalization of the effective optical paths and by the acquisition time δ_{at} . Using the relativistic Lorentz equations, one finds [20,21]

$$\beta_{t,\max} = \sqrt{1 + \frac{(1 - \beta^2)[1 - \rho^2]}{[\rho + \frac{\pi\beta\delta t}{T} \sin \chi]^2}}, \quad (6)$$

where χ is the unknown angle that the relative velocity vector of the preferred frame with respect to the laboratory frame makes with the earth's rotation axis, β is its modulus, T is the earth rotation day, and $\rho = \frac{d_{AB}}{\Delta d}$, where d_{AB} is the optical path between points A and B in the laboratory frame. The parameter δt ($\delta t/T \ll 1$) in Eq. (6) is usually assumed to coincide with the acquisition time δ_{at} needed for a complete measurement of S_{\max} , but this is not correct. Indeed, if t_i ($i = 1, 2$) are the daily times where the orthogonality condition

$\vec{\beta} \cdot \vec{AB} = 0$ is satisfied, the superluminal model predicts that no communication is possible in the time intervals $I_i = [t_i - \delta t/2, t_i + \delta t/2]$ if $\beta_t < \beta_{t,\max}$ [20,21]. Unfortunately, times t_i are unknown and the acquisitions cannot be synchronized with them. One can be sure that a full acquisition interval δ_{at} is contained in the unknown I_i interval only if $\delta_{at} \leq \delta t/2$. This means that the parameter δt in Eq. (6) is actually given by

$$\delta t = 2 \delta_{at}. \quad (7)$$

Due to the rotation of the earth around its axis and to the revolution motion around the sun, both β and χ depend on time. Since the breaking of quantum mechanics should occur at times t_1 and t_2 where the orthogonality condition $\vec{\beta} \cdot \vec{AB} = 0$ is satisfied, strictly speaking, the β and χ values appearing in Eq. (6) should correspond to the values of these parameters at these special times. However, in our experimental conditions the variations of β and χ due to earth's motion can be disregarded and these parameters can be assumed to be constant in Eq. (6).¹

Some experimental tests of the superluminal models have been reported in the literature, but so far no evidence for a violation of the quantum mechanics predictions has been found and only lower bounds $\beta_{t,\max}$ for the superluminal velocity β_t have been established [19–22]. In Ref. [22] the locality and freedom-of-choice loopholes were also addressed. Here we report the results of an experiment where the loopholes above are not taken into account but the maximum detectable velocity of the superluminal communications is increased by about two orders of magnitude for any value of β and χ . According to [23], we here test the assumption that quantum correlations are due to supraluminal influences of a first event on a second event.

II. EXPERIMENT

A. Apparatus and procedures

Our experimental apparatus, the procedures used to get very small values of the basic experimental parameters ρ and δt , and the experimental uncertainties have been described in detail in a previous paper [19] and thus here we will recall only the main features.

To reach a high value of $\beta_{t,\max}$, one has to make the parameters ρ and δt in Eq. (6) as small as possible. We get a small value of $\rho = \frac{d_{AB}}{\Delta d}$ performing our measurements in the so-called east-west gallery of the European Gravitational Observatory (EGO) [24] of Cascina ($d_{AB} \approx 1200$ m) and using an interferometric method to equalize the optical paths d_A

¹In our experiment $\rho = 1.83 \times 10^{-7}$ and $\delta t = 0.494$ s (see Sec. II A), leading to $\frac{\pi\beta\delta t}{T} \sin \chi \ll \rho$ if $\beta \ll 10^{-2}$. Then $\beta_{t,\max}$ is virtually independent of β if $\beta < 10^{-4}$ (see, for instance, curve a in Fig. 7). The modulus of the adimensional earth rotation velocity around its axis is $\beta_r \approx 1.5 \times 10^{-6}$ and that of the revolution motion around the sun is $\beta_{\text{rev}} \approx 10^{-4}$, which leads to $|\Delta\beta_{\text{rev}}| < 2.2 \times 10^{-6}$ during the whole measurement time (8 days). Then the variation $\Delta\beta$ of the modulus of the relative adimensional velocity of the preferred frame due to the earth's motion satisfies the condition $|\Delta\beta| \lesssim 5 \times 10^{-6}$ during the whole measurement time (approximately 8 days) and thus it does not affect appreciably $\beta_{t,\max}$ in Eq. (6) for any β value.

and d_B ($d_A \approx d_B \approx 600$ m). The final uncertainty Δd of the equality of the effective optical paths is due to many error sources including (in order of relevance) the finite thickness of the polarizing layers, the air dispersion, the uncertainty of the interferometric measurement, and the wave-packet width. In the present experiment we collect the entangled photons emitted over a solid angle having a 0.8° aperture and then, using the phase-matching equations for our β barium borate (BBO) crystals, we get a bandwidth $\Delta\lambda \approx 100$ nm that corresponds to a width $\frac{\lambda^2}{\Delta\lambda} \approx 6.4$ μm of the emitted wave packets that is negligible with respect to the other sources of uncertainty. As shown in Ref. [19], the estimated uncertainty in our experiment is $\Delta d \approx 0.22$ mm. To reduce the acquisition time we need a high-intensity source of entangled photons in a sufficiently pure entangled state. We get this by using the compensation procedures developed by Kwiat and co-workers [25–27] and developing a proper optical configuration that ensures low losses of entangled photons along the gallery. Unfortunately, the EGO gallery is not aligned along the east-west axis but makes the angle $\gamma = 18^\circ = \pi/10$ with it. Then one easily infers that the orthogonality condition $\vec{\beta} \cdot \vec{AB} = 0$ can be never satisfied if the velocity vector of the preferred frame makes a polar angle $\chi < \gamma = \pi/10$ or $\chi > \pi - \gamma = 9\pi/10$ with respect to the earth's rotation axis. This means that our experiment is virtually insensitive to the fraction $\Omega/4\pi = \int_0^\gamma \sin\theta d\theta < 5\%$ of all the possible alignments of the preferred frame velocity vector. For a detailed analysis of the case $\gamma \neq 0$ we refer the reader to Ref. [20]. Note that the reference frame of the cosmic microwave background ($\chi \approx 97^\circ$) is accessible in experiment. Equation (6) was obtained under the assumption that the experiment is aligned along the east-west axis ($\gamma = 0$) but for $\gamma > 0$ and $\pi - \gamma \geq \chi \geq \gamma$ it has to be replaced by [20]

$$\beta_{t,\max} = \sqrt{1 + \frac{(1 - \beta^2)[1 - \rho^2]}{[\rho + A \frac{\pi\beta\delta t}{T}]^2}}, \quad (8)$$

where the coefficient A is defined as

$$A = \sqrt{\sin^2 \chi \cos^2 \gamma - \cos^2 \chi \sin^2 \gamma}. \quad (9)$$

The velocity $\beta_{t,\max}$ greatly decreases out of the interval $\pi - \gamma \geq \chi \geq \gamma$ [20].

A schematic view of the experimental apparatus is shown in Fig. 2. A pump laser beam at a wavelength $\lambda_p = 406.3$ nm is generated by the 220-mW laser diode shown at the top right in Fig. 2. The pump beam passes through an achromatic lens, a Glan-Thompson polarizer, a motorized $\lambda/2$ plate, a motorized Babinet-Soleil compensator, and a quartz plate C . Then it is reflected by a mirror, passes through a 565-nm short-pass dichroic mirror (Chroma T565spxe), and is focused (spot diameter equal to 0.6 mm) at the center of two thin (thickness approximately equal to 0.56 mm) adjacent, crossed, BBO, nonlinear optical crystal plates (29.05° tilt angle) cut for type I phase matching [28]. The BBO plates have the optical axes lying in the horizontal and vertical planes, respectively. The $\lambda/2$ plate aligns the polarization of the incident pump beam at 45° with respect to the horizontal axis. The quartz plate C compensates for the effects due to the low coherence of the pump beam (a coherence length of approximately 0.2 mm) [27].

Down-conversion leads to two outgoing beams of entangled photons at the average wavelength $\lambda = 2\lambda_p = 812.6$ nm that mainly propagate at two symmetric angles ($\pm 2.4^\circ$) with respect to the normal to the crossed BBO plates. A proper adjustment of the optical dephasing induced by the Soleil-Babinet compensator provides the polarization entangled state in Eq. (1). The entangled beams deviate in opposite directions along the EGO gallery by two right-angle prisms (R_A and R_B) and pass through the BBO compensating plates C_A and C_B . The compensating plates C , C_A , and C_B of Kwiat and co-workers are used to get a high-intensity source of entangled photons ($N_{\text{tot}} \approx 23\,000$ coincidences/s) in an entangled state of sufficient purity [25–27]. The entangled beams, propagating in opposite directions, impinge on polarizers P_A and P_B at a distance of about 600 m from the source. Our experiment requires the equalization of the optical paths d_A and d_B between the source of the entangled photons and polarizers P_A and P_B and needs stable coincidence counts during the whole measurement time (approximately 8 days). Both these requirements are satisfied using four reference beams at wavelength $\lambda_R = 681$ nm that are utilized to align the optical system, to equalize the optical paths, and to compensate for the deviations of the entangled beams due to the air refractive index gradients induced by sunlight on the top of the gallery. The four reference beams are obtained starting from the collimated beam emitted by the 3-mW superluminescent diode shown at the top left in Fig. 2. The beam passes through a beam displacer (Thorlabs BDY12U) that splits the incident beam into two parallel beams (I and II) at a relative distance of 1.2 mm. Beam I is represented by a solid line in the figure and beam II by a dashed line. Beams I and II are focused (spot diameter approximately equal to 0.3 mm) orthogonally on a transmission phase grating that mainly produces two diffracted beams at diffraction angles $\pm 2.43^\circ$ that are virtually coincident with the average emission angles of the entangled photons ($\pm 2.42^\circ$). An achromatic lens (150-mm focal length) projects on the crossed BBO plates a 1:1 image of the spots of beams I and II occurring on the grating. The spot of beam I is centered within approximately ± 0.03 mm with respect to the pump beam spot where the entangled photons are generated (the source of the entangled photons). Then beams I outgoing from the crossed BBO plates virtually follow the same paths as the entangled beams. The whole system described above lies on an optical table and is enclosed in a large box that ensures a fixed temperature $T = 24^\circ\text{C} \pm 0.1^\circ\text{C}$ by circulation of Parafllu fluid. Two 80-W fans ensure a sufficient temperature uniformity. The entangled beams and the reference beams are collected by large-diameter (15-cm) achromatic lenses L_A and L_B that have been built to have the same focal length at the wavelengths of the reference and the entangled beams (6.00 m at $\lambda_R = 681$ nm and $\lambda = 812.6$ nm). These beams propagate along the gallery arms and impinge on two identical achromatic lenses L'_A and L'_B at a distance approximately 600 m from the source of the entangled photons. Real 1:1 images (0.6 mm wide) of the source and of the spot of beam I occurring on the crossed BBO plates are produced at the centers of the linear polarizers layers P_A and P_B (Thorlabs LPNIR). Beams II slightly deviate due to lenses L_A and L_B and impinge on two diffusing screens put adjacent to lenses L'_A and L'_B . The diffused light outgoing from each screen is collected by a webcam connected to a personal

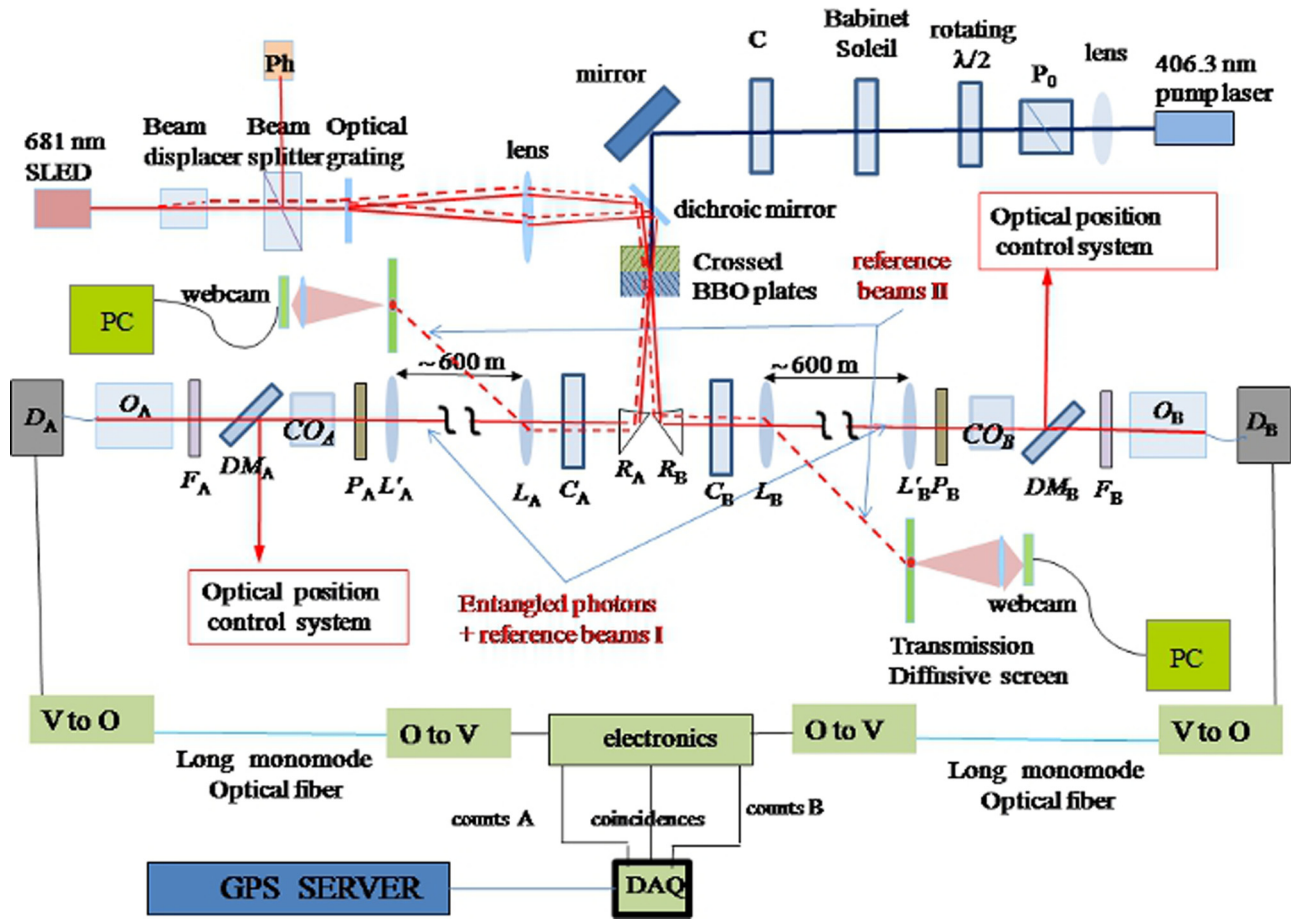


FIG. 2. Schematic view of the experimental apparatus. Note that the figure is not to scale and, in particular, the distances between lenses L_A and L_B and lenses L'_A and L'_B (approximately 600 m) are much larger than all the other distances. To simplify the drawing some details have not been included in the figure. The 220-mW pump beam with wavelength $\lambda_p = 406.3$ nm (blue thick solid line in the figure) is polarized by the polarizer P_0 and the $\lambda/2$ plate. The Babinet-Soleil compensator introduces a variable optical dephasing between the horizontal and vertical polarizations. Here C , C_A , and C_B are anisotropic compensator plates used to get a high-intensity source of entangled photons with a sufficient fidelity and R_A and R_B are right angle prisms. The pump beam is focused at the center of two crossed adjacent BBO plates (29.05° tilt angle) where entangled photons having wavelength $\lambda = 812.6$ nm are generated and emitted at the angles $\pm 2.42^\circ$ with respect to the pump laser beam. Further, L_A , L_B , L'_A , and L'_B are specially designed 15-cm-diam achromatic lenses aligned along the EGO gallery and having a 6.00-m focal length at both the 812.6- and 681-nm wavelengths. In addition, P_A and P_B are absorption polarizing filters; O_A , O_B , CO_A , and CO_B are systems of lenses; DM_A and DM_B are dichroic mirrors; F_A and F_B are sets of adjacent optical filters; and D_A and D_B are photon-counting detectors. The superluminescent diode (SLED) having wavelength $\lambda_R = 681$ nm and coherence length $28.1 \mu\text{m}$, the beam displacer, and the optical grating are used to produce two reference beams in each arm of the EGO gallery (solid and dashed red lines) as discussed in the text. Here V to O denotes electronic systems that transform the output voltage pulses produced by the photon-counting detectors into optical pulses, while O to V transforms the optical pulses into voltage pulses. Also, DAQ is a National Instruments CompactDAQ that provides a real-time acquisition of coincidences.

computer (PC) and a LABVIEW program calculates the position of the diffusing spot. The daily displacements of the above spots (up to 1.2 m in a summer day) due to air refractive index gradients induced by sunlight are compensated using a proper feedback where lenses L_A and L_B are moved orthogonally to their optical axes to maintain fixed the position of the spots on the diffusing screens (see Sec. 2.2 in Ref. [19] for details). This procedure ensures that beams I and thus the entangled beams remain virtually centered with respect to lenses L'_A and L'_B . The reference beams I outgoing from polarizers P_A and P_B are almost fully reflected by the long-pass dichroic mirrors DM_A and DM_B (Chroma T760lpxr) and enter the optical position control systems that measure the position and the astigmatism of the beam spots on the polarizers. Using a LABVIEW program

operating in a PC, lenses L'_A and L'_B are moved orthogonally to their optical axes to maintain the spot position at the center of the polarizers within ± 0.4 mm during the whole measurement time. An other program controls the astigmatism of the images using the variable-focus cylindrical lenses CO_A and CO_B . The equalization of the optical paths d_A and d_B is obtained by exploiting the beams I that are partially reflected by the polarizing layers P_A and P_B and that return, producing interference on the photodetector (Ph) shown on the top left in Fig. 2. Details on the feedback procedures and on the interferometric method can be found in Secs. 2.2 and 2.3 of Ref. [19], respectively. Each of the entangled photons beams outgoing from the two polarizers passes through the long-pass dichroic mirror (DM_A or DM_B in the figure) and a filtering set (F_A or F_B in the figure) made

by two long-pass optical filters (Chroma ET765lp filters, $\lambda_c = 765$ nm) that stop the reference 681-nm beams and a bandpass filter (Chroma ET810/40m, $\lambda = 810$ nm \pm 20 nm). Then each beam is focused by a system of optical lenses (O_A or O_B) on a 200- μ m multimode optical fiber having a large numerical aperture (0.39) connected to a Perkin Elmer photons-counter module. The output pulses of the photons counters are transformed into optical pulses (using the LCM155EW4932-64 modules of Nortel Networks) that propagate in two monomode optical fibers toward the central optical table where the entangled photons are generated. Finally, the optical pulses are transformed again into electric pulses and sent to an electronic coincidence circuit. An electronic counter connected to a National Instruments CompactDAQ counts the Alice pulses N_A , the Bob pulses N_B , and the coincidences pulses N .

B. Fast acquisition procedure

In our preliminary experiment [19], the measurements of the probabilities appearing in Eq. (2) were made sequentially: A PC connected to precision stepper motors rotated polarizers P_A and P_B up to reach the first couple of angles α and β appearing in Eq. (2) ($\alpha = 45^\circ$ and $\beta = 67.5^\circ$) and the corresponding coincidences $N(\alpha, \beta)$ were acquired with an acquisition time of 1 s; then the successive couple of α and β angles was set and the corresponding coincidences were acquired and so on. When all eight contributions $N(\alpha, \beta)$ appearing in Eqs. (2) and (4) were obtained, the program calculated S_{\max} . This procedure needed many consecutive rotations of the polarizers before a single value of S_{\max} was obtained leading to a long acquisition time interval $\delta_a t \approx 100$ s for each measurement of S_{\max} . To greatly reduce $\delta_a t$ and increase the maximum detectable adimensional velocity $\beta_{t, \max}$, we exploit here the daily periodicity of the investigated phenomenon and we measure each of the four contributions appearing in Eq. (2) in successive daily experimental runs. This procedure allows us to set the polarization angles α and ξ only one time each day before starting the measurement of P_i . Then any retardation due to the polarizer rotation is avoided. Furthermore, the PC used in our previous experiment has been replaced here by a National Instruments CompactDAQ where a real-time LABVIEW program runs. This procedure ensures a full continuity of the acquisitions and a constant acquisition time. The obtained experimental values of the basic parameters ρ (see the analysis at the end of Sec. 3 in [19]) and δt appearing in Eq. (6) are

$$\rho = 1.83 \times 10^{-7}, \quad \delta t = 2\delta_a t = 0.494 \text{ s}, \quad (10)$$

which provide $\beta_{t, \max}$ values about two orders of magnitude higher than the those obtained in previous experiments. A Global Positioning System (GPS) Network Time Server (TM2000A) provides the actual Coordinated Universal Time (UTC) [29,30] with an absolute accuracy better than 1 ms also if the connection to the satellites is lost up to a time of 80 h. Since the investigated phenomenon is related to the earth's rotation, we synchronize the acquisitions with the earth's rotation time $t = \theta \times 240$ s, where θ is the Earth Rotation Angle [31] expressed in degrees. The earth's rotation time is the modern alternative to the sidereal time and it is given by $t = 86400 \times (\text{TJ mod } 1)$, where mod represents the modulo operation and $\text{TJ} = [a_1 + b_1 \times (\text{Julian UT1 day} -$

2451545.0)], with $a_1 = 0.7790572732640$ days and $b_1 = 1.00273781191135448$. The Julian UT1 day is strictly related to the UT1 time that takes into account the nonuniformity of the earth's rotation velocity and thus does not coincide with the UTC atomic time provided by the GPS. The IERS Bulletin A [32] provides the value of the daily difference $\Delta = \text{UT1} - \text{UTC}$ and thus the UT1 and the earth's rotation time can be calculated. We decide to start each acquisition run at the Greenwich earth rotation time $t = 0$.

The successive steps of the fully automated procedure are as follows.

(i) The GPS Greenwich UTC time and the UT1-UTC value are acquired and then the Greenwich earth rotation time t is calculated. Successively, the UTC time that corresponds to the next zero value of the Greenwich earth rotation time is calculated.

(ii) Two hours before the occurrence of $t = 0$, we measure the total number of couples of entangled photons N_{tot} . The program rotates the P_A and P_B polarizers and sets successively the α and ξ angles that appear in the expression of the total number of incident entangled couples N_{tot} in Eq. (4). For each setting of the polarizer angles, the coincidences are measured for a sufficiently long acquisition time interval (100 s) to made negligible the counts' statistical noise with respect to others noise sources. The spurious statistical coincidences $N_S = N_A \times N_B \times T_p / \delta_a t$ are subtracted, where T_p is the pulse duration time and $\delta_a t$ is the acquisition time interval. The value $T_p = 29.2$ ns is obtained from a calibration procedure where coincidences between totally uncorrelated photons are detected. Finally, the total number of entangled photons N_{tot} is calculated using Eq. (4).

(iii) At the end of these preliminary measurements, the polarizer angles are set at the values $\alpha = 45^\circ$ and $\xi = 67.5^\circ$ appearing in the first contribution P_0 in Eq. (2). Then the acquisition of the coincidences starts at the Greenwich earth rotation time $t = 0$. The duration of a complete acquisition run is $T_0 = 36$ earth rotation hours, which corresponds to about 35 h, 54 min, and 7 s in the standard UTC time. Here 2^{19} successive acquisitions are made in each acquisition run with the acquisition time interval $\delta_a t = \frac{T_0}{2^{19}} \simeq 246.517461$ ms (in standard UTC unities). Note that, due to the daily small changes of the UT1 – UTC difference, $\delta_a t$ exhibits small daily variations (the maximum variation was approximately equal to 0.000001 ms in the whole measurement time). To ensure a time precision better than 1 ms, the microsecond internal counter of real-time LABVIEW is used and the GPS server is interrogated every 5 min. Furthermore, a suitable subroutine partially corrects (within 0.1 ms) time errors introduced by the microsecond quantization of the data acquisition (DAQ) clock.²

²Due to the microseconds quantization of the DAQ clock, the acquisition time interval $\delta_a t = 246517 \mu\text{s}$ is smaller than $T_0/2^{19} = 246517.46170157 \dots \mu\text{s}$ by the quantity $\Delta_q t = 0.46170157 \dots \mu\text{s}$. Then the i th acquisition interval is shifted by $(i-1)\Delta_q t$ with respect to the correct value $(i-1)\delta_a t$. As soon as this shift becomes greater than $100 \mu\text{s}$ (for a given i), the LABVIEW program increases the acquisition time of the i th interval to $\delta_a t + 100 \mu\text{s}$. The same procedure is repeated whenever the successive shift just exceeds the

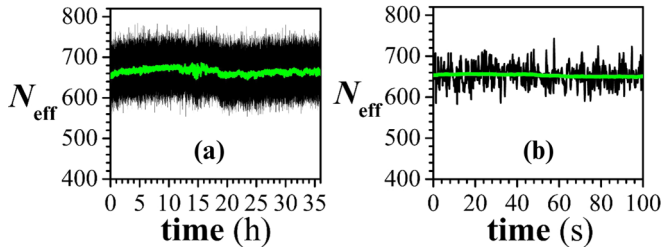


FIG. 3. (a) Example of the effective coincidences (true plus spurious) versus the Greenwich earth rotation time. The 2^{19} points are connected by black lines leading to the resulting black region in the figure. The acquisition time of coincidences is $\delta_a t \approx 0.246$ s in standard UTC units. The green solid line is the result of smoothing averaging over 200 adjacent points. The slow variations in the smoothing curve are caused by residual noise due to sunlight on the top of the gallery. (b) Detail of the coincidences over 100 s.

(iv) At the end of the first acquisition run, the program calculates the 2^{19} values of P_0 and sets the second couple of angles α and ξ appearing in the P_1 term in Eq. (2). Then steps (iii) and (iv) are repeated until all probabilities P_i appearing in Eq. (2) are obtained. To appreciably reduce the residual spurious effects due to air turbulence induced by sunlight on the top of the gallery, all the measurements were performed during the 2017 autumn season starting at earth rotation hour 0 of October 24 and stopping at earth rotation hour 12 of October 31.

III. RESULTS AND CONCLUSION

Figure 3(a) shows an example of the effective coincidences (true plus spurious) N_{eff} versus the Greenwich earth rotation time during a single run. The green solid line is the result of a smoothing obtained averaging over 200 adjacent points; a detail of the coincidences over 100 s is shown in Fig. 3(b). The small slow changes that are visible in the smoothing curve are strictly related to the daily small residual displacements of the entangled photons beams induced by sunlight. The greater contribution to noise in our experiment is the statistical counts noise, while the other noise sources are virtually negligible. This is evident if we eliminate the slow fluctuations plotting the filtered coincidences $N_{\text{filt}} = N_{\text{eff}} - N(\text{smoothing}) + \langle N_{\text{eff}} \rangle$. Figure 4(a) shows N_{filt} versus the Greenwich earth rotation time, while Fig. 4(b) shows the corresponding probability distribution P (black points). We emphasize here that the solid green line in Fig. 4(b) is not a best fit, but it is the normal Gaussian function with parameters σ and $\langle N_{\text{filt}} \rangle$ that are predicted by the statistics of counts and are given by $\sigma^2 = \langle N_{\text{filt}} \rangle = 665.042$. Figures 5(a)–5(d) show the probabilities $P_i = P(\alpha_i, \xi_i) = \frac{N(\alpha_i, \xi_i)}{N_{\text{tot}}}$ obtained in the successive runs where the spurious coincidences $N_S = N_A \times N_B \times T_p / \delta_a t$ have been subtracted but no filtering was performed. The black region represents the measured values, the solid green line represents the average value, and the green dotted line represents the value

100- μ s value. In such a way the maximum residual shifts are always lower than approximately 100 μ s and thus are negligible with respect to the width $\delta_a t = 246517 \mu$ s of each acquisition interval.

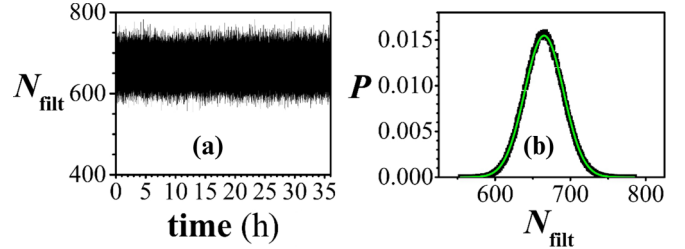


FIG. 4. (a) Filtered coincidences $N_{\text{filt}} = N_{\text{eff}} - N(\text{smoothing}) + \langle N_{\text{eff}} \rangle$ where the slow instrumental drift of the average value in Fig. 3 has been subtracted. The acquisition time of coincidences is $\delta_a t \approx 0.246$ s and the total number of acquisitions is 2^{19} . (b) Probability distribution of the coincidences (black points). The solid green curve does not represent a best fit but it is the normal distribution predicted by the statistic theory of counts having $\sigma^2 = \langle N_{\text{filt}} \rangle = 665.042$ with no free parameters.

predicted by quantum mechanics for the pure entangled state in Eq. (1) (fidelity $F = 1$). The discrepancy between the solid and dotted lines indicates that our entangled state is not completely pure ($F < 1$) or that some systematic noise is present. In the simplest and rough assumption that the breakdown of quantum correlations occurs with exactly the earth rotation periodicity, one could calculate an S_{max} value at each earth rotation time by substituting the P_i contributions of Fig. 5 measured at the same earth rotation time t during different experimental runs into the theoretical expression of S_{max} in Eq. (2).

With this procedure we get the results shown in Fig. 6(a) (black region) and the corresponding frequency distribution

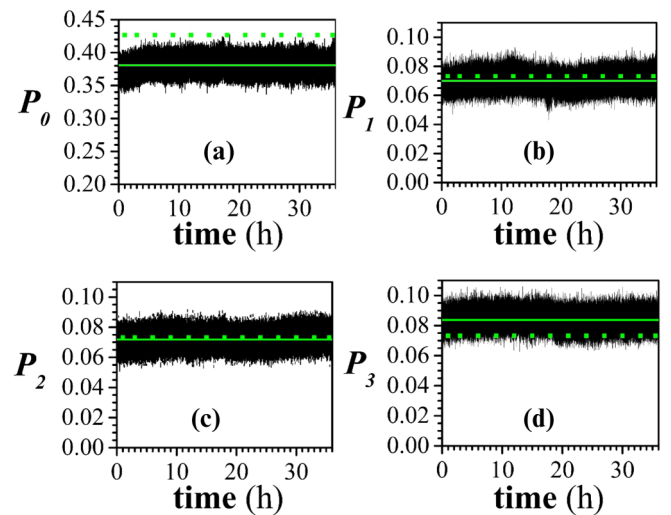


FIG. 5. Probabilities (a) P_0 , (b) P_1 , (c) P_2 , and (d) P_3 measured in successive runs versus the Greenwich earth rotation time. The 2^{19} measured values are connected by straight lines leading to the resulting black regions in the figure. The acquisition time is $\delta_a t \approx 0.246$ s. The green solid lines represent the average values of the measured probabilities: $\langle P_0 \rangle = 0.38087$, $\langle P_1 \rangle = 0.06999$, $\langle P_2 \rangle = 0.07187$, and $\langle P_3 \rangle = 0.08378$. The green dotted lines correspond to the values predicted by quantum mechanics for a pure entangled state: $P_0 = 0.4267$ and $P_1 = P_2 = P_3 = 0.0732$. The difference between dotted and solid lines indicates that our state is not a pure entangled state or that some instrumental noise occurs.

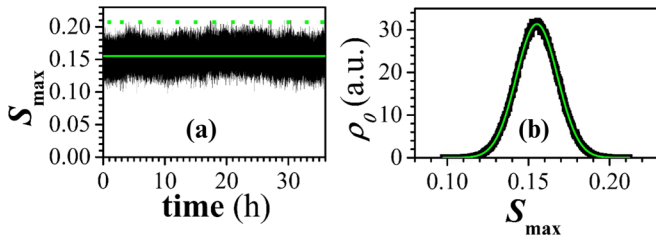


FIG. 6. (a) Parameter S_{\max} versus the earth rotation time obtained using the relation $S_{\max}(t) = P_0(t) - P_1(t) - P_2(t) - P_3(t)$. The green solid line is the average value $\langle S_{\max} \rangle = 0.15523$, while the green dotted line represents the quantum mechanics average value $\langle S_{\max} \rangle = 0.207$ characterizing the pure entangled state in Eq. (1). The difference between dotted and solid lines indicates that our state is not a pure entangled state. However, the average value $\langle S_{\max} \rangle = 0.15523$ is sufficiently greater than zero to allow an accurate test of the Bell inequality. (b) Frequency distribution ρ_0 of the 2^{19} measured values of S_{\max} in arbitrary units. The full green curve is the Gaussian fit with standard deviation $\sigma = 0.01272$ and $\langle S_{\max} \rangle = 0.15523$.

ρ_0 shown in Fig. 6(b), where black points represent the experimental results and the solid green line is the best fit with the Gaussian function $A \exp\left[-\frac{(S_{\max} - \langle S_{\max} \rangle)^2}{(2\sigma^2)}\right]$ with standard deviation $\sigma = 0.01272$ and $\langle S_{\max} \rangle = 0.15523$. The green solid line in Fig. 6(a) shows the average value $\langle S_{\max} \rangle$ and the green dotted line is the value $S_{\max} = 0.2071$ predicted by quantum mechanics for the pure entangled state in Eq. (1) ($F = 1$). No breakdown of S_{\max} to zero is visible in Fig. 6(a) and the lowest experimental values of S_{\max} are at more than seven standard deviations from the maximum value $S_{\max} = 0$ predicted by local variables models. However, the analysis above is not sufficient to conclude that no superluminal effect is present. In fact, the breakdown of the quantum mechanics correlations is predicted to occur at the two times where $\vec{\beta} \cdot \vec{A}\vec{B} = 0$, where $\vec{\beta}$ is the adimensional velocity vector of the preferred frame with respect to earth's laboratory frame. Due to the revolution motion of the earth around the sun and other motions (precession and nutation of the earth's axis), the vector $\vec{\beta}$ does not return exactly at the same orientation with respect to the laboratory frame after one earth rotation day. The orthogonality condition is not satisfied exactly at the same earth rotation times in different earth rotation days, but some unknown time shift can occur (shifts lower than a few minutes per day can be expected). A rigorous test of the v -causal models requires a completely different analysis of the experimental data. We denote by t_{i1} and t_{i2} the two unknown times during the i th measurement run ($i = 0 - 3$) where the orthogonality condition $\vec{\beta} \cdot \vec{A}\vec{B} = 0$ is satisfied and by $P_i(t_{ij})$, with $i = 0 - 3$ and $j = 1, 2$, the corresponding probabilities measured at these times. According to the v -causal models, if $\beta_t < \beta_{t,\max}$ all or some of these probabilities should be different from the quantum mechanics values and thus the correlation parameters

$$S_{\max}(j) = P_0(t_{0j}) - \sum_{i=1}^3 P_i(t_{ij}), \quad (11)$$

with $j = 1, 2$, should satisfy the Bell inequality $S_{\max}(j) \leq 0$ if $\beta_t < \beta_{t,\max}$.

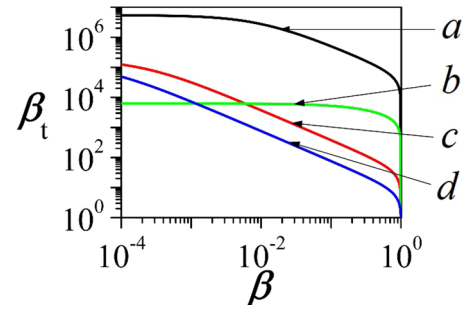


FIG. 7. Curve a shows the $\beta_{t,\max}$ values obtained in our experiment using Eq. (8) ($\rho = 1.83 \times 10^{-7}$, $\delta t = 2$, $\delta_a t = 0.494$ s, and $\gamma = 18^\circ$) versus the unknown adimensional velocity β of the preferred frame for the unfavorable case $\chi = \frac{\pi}{2}$, curve b is the result obtained in Ref. [21] ($\rho = 1.6 \times 10^{-4}$, $\delta t = 2$, $\delta_a t = 8$ s, and $\gamma = 0^\circ$), curve c is the result obtained in Ref. [20] ($\rho = 5.4 \times 10^{-6}$, $\delta t = 2$, $\delta_a t = 720$ s, and $\gamma = 5.9^\circ$), and curve d is the result obtained in Ref. [22] ($\rho = 7.3 \times 10^{-6}$, $\delta t = 2$, $\delta_a t = 3600$ s, and $\gamma = 0^\circ$). Note that only in the case of curve d also the locality and the freedom-of-choice loopholes were addressed.

We do not know times t_{ij} and we cannot calculate $S_{\max}(j)$, but it is obvious from Eq. (11) that $S_{\max}(j) \geq S = \min(P_0) - \max(P_1) - \max(P_2) - \max(P_3)$, where $\min(P_i)$ and $\max(P_i)$ denote the absolute minimum and maximum measured values of P_i , respectively. From the data in Fig. 5 we get $S = 0.04237$ and thus $S_{\max}(j) \geq 0.04237 \approx 3.3\sigma$. This means that the probability that a value of $S_{\max}(j)$ lower than or equal to zero could be compatible with our measured values is $p \leq \frac{1}{2} \operatorname{erfc}\left[\frac{0.04237}{(\sqrt{2}\sigma)}\right] = 4.3 \times 10^{-4}$, where $\operatorname{erfc}(x)$ is the complementary error function. The superluminal models predict that at the least two breakdowns of S_{\max} must occur in the time of 36 h and thus the probability that both these breakdowns happen here is $p \leq p^2 \sim 2 \times 10^{-7}$. Then we can conclude that no evidence for the presence of superluminal communications is found and only a higher value of the lower bound $\beta_{t,\max}$ can be established. Substituting the experimental values $\rho = 1.83 \times 10^{-7}$ and $\delta t = 2$, $\delta_a t = 0.494$ s in Eq. (8), one obtains $\beta_{t,\max}$ as a function of the unknown modulus β ($\beta < 1$) of the adimensional velocity of the preferred frame and of the angle χ with respect to the earth's rotation axis. We recall that Eq. (8) holds only if the angle χ is inside the interval $[\gamma, \pi - \gamma]$ where $\gamma = \pi/10$ rad, while $\beta_{t,\max}$ sharply decreases out of this interval [20]. According to Eq. (8), $\beta_{t,\max}$ reaches the maximum value at the borders $\chi = \gamma$ and $\chi = \pi - \gamma$ and the minimum value at $\chi = \pi/2$. The upper curve in Fig. 7 shows our $\beta_{t,\max}$ versus the unknown adimensional velocity β of the preferred frame in the unfavorable case $\chi = \pi/2$. For preferred frame velocities comparable to those of the cosmic microwave background frame ($\beta \approx 10^{-3}$), the corresponding lower bound is $\beta_{t,\max} \approx 5 \times 10^6$. The lower curves represent the experimental values of $\beta_{t,\max}$ obtained in the previous experiments [20–22]. No breakdown of quantum correlations has been observed and thus we can infer that either the superluminal communications are not responsible for quantum correlations between entangled particles or their adimensional velocities are greater than $\beta_{t,\max}$. Finally, it should be noted that the possibility remains open that $\beta_t < \beta_{t,\max}$, but the vector $\vec{\beta}$

makes a polar angle $\chi < \gamma = \pi/10$ or $\chi > \pi - \gamma = 9\pi/10$ with the earth's rotation axis.

ACKNOWLEDGMENTS

We acknowledge the Fondazione Pisa for financial support. We acknowledge the EGO and VIRGO staffs that made

possible the experiment and, in particular, F. Ferrini, F. Carbognani, A. Paoli, and C. Fabozzi. We are especially grateful to M. Bianucci (Physics Department, Università di Pisa) and to S. Cortese (VIRGO) for their invaluable and continuous contribution to the solution of many electronic and informatic problems. Finally, we acknowledge N. Gisin for helpful comments and T. Faetti for helpful suggestions on real-time procedures.

-
- [1] A. Einstein, B. Podolsky, and N. Rosen, *Phys. Rev.* **47**, 777 (1935).
- [2] J. S. Bell, *Physics* **1**, 195 (1964).
- [3] J. F. Clauser, M. A. Horne, A. Shimony, and R. Holt, *Phys. Rev. Lett.* **23**, 880 (1969).
- [4] J. F. Clauser and M. A. Horne, *Phys. Rev. D* **10**, 526 (1974).
- [5] A. Aspect, J. Dalibard, and G. Roger, *Phys. Rev. Lett.* **49**, 1804 (1982).
- [6] B. Hensen, H. Bernien, A. E. Dréau, A. Reiserer, N. Kalb, M. S. Blok, J. Ruitenbergh, R. F. L. Vermeulen, R. N. Schouten, C. Abellán, W. Amaya, V. Pruneri, M. W. Mitchell, M. Markham, D. J. Twitchen, D. Elkouss, S. Wehner, T. H. Taminiau, and R. Hanson, *Nature (London)* **526**, 682 (2015).
- [7] M. Giustina *et al.*, *Phys. Rev. Lett.* **115**, 250401 (2015).
- [8] L. K. Shalm *et al.*, *Phys. Rev. Lett.* **115**, 250402 (2015).
- [9] W. Rosenfeld, D. Burchardt, R. Garthoff, K. Redeker, N. Ortewel, M. Rau, and H. Weinfurter, *Phys. Rev. Lett.* **119**, 010402 (2017).
- [10] N. Gisin, in *Quantum Theory: A Two-Time Success Story: Yakir Aharonov Festschrift*, edited by D. C. Struppa and J. M. Tollaksen (Springer Milan, Milano, 2014), pp. 185–203.
- [11] *The Ghost in the Atom: A Discussion of the Mysteries of Quantum Physics*, edited by P. C. W. Davies and J. R. Brown (Cambridge University Press, Cambridge, 1986).
- [12] P. H. Eberhard, in *Quantum Theory and Pictures of Reality: Foundations, Interpretations, and New Aspects*, edited by W. Schommers (Springer, Berlin, 1989), p. 169.
- [13] D. Bohm and B. J. Hiley, *The Undivided Universe: An Ontological Interpretation of Quantum Mechanics* (Routledge, London, 1993).
- [14] B. Cocciaro, *Phys. Essays* **26**, 531 (2013).
- [15] B. Cocciaro, *J. Phys.: Conf. Ser.* **626**, 012054 (2015).
- [16] J. Bancal, S. Pironio, A. Acín, Y. Liang, V. Scarani, and N. Gisin, *Nat. Phys.* **8**, 867 (2012).
- [17] T. J. Barnea, J.-D. Bancal, Y.-C. Liang, and N. Gisin, *Phys. Rev. A* **88**, 022123 (2013).
- [18] A. Aspect, in *Quantum (Un)speakables: From Bell to Quantum Information*, edited by R. A. Bertlmann and A. Zeilinger (Springer, Berlin, 2002).
- [19] B. Cocciaro, S. Faetti, and L. Fronzoni, *J. Phys.: Conf. Ser.* **880**, 012036 (2017).
- [20] D. Salart, A. Baas, C. Branciard, N. Gisin, and H. Zbinden, *Nature (London)* **454**, 861 (2008).
- [21] B. Cocciaro, S. Faetti, and L. Fronzoni, *Phys. Lett. A* **375**, 379 (2011).
- [22] J. Yin, Y. Cao, H.-L. Yong, J.-G. Ren, H. Liang, S.-K. Liao, F. Zhou, C. Liu, Y.-P. Wu, G.-S. Pan, L. Li, N.-L. Liu, Q. Zhang, C.-Z. Peng, and J.-W. Pan, *Phys. Rev. Lett.* **110**, 260407 (2013).
- [23] D. Salart, A. Baas, C. Branciard, N. Gisin, and H. Zbinden, [arXiv:0810.4607](https://arxiv.org/abs/0810.4607).
- [24] European Gravitational Observatory, <https://www.ego-gw.it/>
- [25] J. Altepeter, E. Jeffrey, and P. Kwiat, *Opt. Express* **13**, 8951 (2005).
- [26] G. M. Akselrod, J. B. Altepeter, E. R. Jeffrey, and P. G. Kwiat, *Opt. Express* **15**, 5260 (2007).
- [27] R. Rangarajan, M. Goggin, and P. Kwiat, *Opt. Express* **17**, 18920 (2009).
- [28] P. G. Kwiat, E. Waks, A. G. White, I. Appelbaum, and P. H. Eberhard, *Phys. Rev. A* **60**, R773 (1999).
- [29] P. K. Seidelmann, B. Guinot, and L. E. Doggett, in *Explanatory Supplement to the Astronomical Almanac*, edited by P. K. Seidelmann (University Science Books, Mill Valley, 1992).
- [30] National Radio Astronomy Observatory, Rick Fisher homepage, <https://www.cv.nrao.edu/~rfisher/>
- [31] I. Ridpath, *A Dictionary of Astronomy*, 2nd ed. (Oxford University Press, Oxford, 2012).
- [32] International Earth Rotation and Reference Systems Service, <https://datacenter.iers.org/>